PROCEEDINGS, 45th Workshop on Geothermal Reservoir Engineering
Stanford University, Stanford, California, February 10-12, 2020
SGP-TR-216

Thermal Considerations of Cement Integrity in Geothermal Wells

Yuxing Wu[1], Harshkumar R. Patel[1], Saeed Salehi[1]

Well Construction Technology Center (WCTC), The University of Oklahoma, Norman, OK, USA

[1]salehi@ou.edu

Keywords: High temperature, Geothermal well, Cement failure, Finite element analysis, Cement integrity

ABSTRACT

Cement sheath, placed between casing and formation, is an important barrier to provide a hydraulic seal and establish zonal isolation, preventing fluid communication in the wellbore. In geothermal wells, the temperature at the bottom hole is high. Thermal stress induced by temperature is one of the major considerations to trigger failure in the cement sheath. In this study, a numerical model was created based on the FORGE geothermal well in Utah to investigate the effect of casing pressure, temperature and thermal related parameters on cement integrity of casing-cement-formation systems. To achieve the object, a 3D finite element numerical model consisting of casing-cement-formation was developed. The model assumed that the cement-casing and cement-formation interfaces are bonded. Maximum and minimum horizontal stresses from FORGE geothermal well drilling reports were applied as far-field tectonic stresses. Elastic modulus and mechanical strength used in the model were obtained through laboratory measurements and research literature. Cylindrical mechanical stresses in the cement (i.e. radial and hoop stress) were analyzed against respective limiting strength to identify failure modes of cement. Sensitivity analysis was conducted to understand the effect of cement properties (i.e. expansion coefficient and conductivity), temperature difference between casing and formation (ΔT), and casing pressure on cement integrity.

Results from sensitivity analysis revealed that for similar percentage change, temperature difference could have more influence on cement integrity compared to wellbore pressure. For the same differential temperature (ΔT) between the wellbore and formation, heat transfer from formation to pipe (temperature of pipe is less than formation) is more detrimental to cement integrity than the opposite scenario (temperature of pipe is higher than formation). In the case of heat flow away from the wellbore, hoop stress in cement is mainly dependent on temperature difference while radial stress is primarily dependent on temperature difference as well as wellbore pressure. In the case of heat flow towards the wellbore, radial stress in the cement is primarily a function of temperature difference and wellbore pressure. Hoop stress on the other hand, is mainly dependent on temperature difference and cement's thermal expansion coefficient. This paper adds novel information to research literature by presenting sensitivity of cement mechanical stresses to thermal parameters. Outcome generated from this work would be applicable to both injection and production wells in geothermal applications. Better understanding of influence of thermal parameters will help improve the cement design and structural integrity.

1. INTRODUCTION

With the depletion of conventional wells, well integrity is increasing becoming a challenging problem. An intact cement sheath between casing and reservoir, because of the extremely low permeability, is an important barrier to maintain zonal isolation and prevent formation fluid flow to an unintended area (Wang and Taleghani 2014, Kimanzi et al. 2019). Based on Schrepper (2015), six common failure modes of cement are shown in **Figure 1**. A worldwide study has shown that more than 380,000 wells from Canada, China, Netherlands, Offshore Norway, UK, and US encountered wellbore integrity issues (Davies et al. 2014). A 2015 survey on technological knowledge gaps for high-pressure and high-temperature (HPHT) oil and gas activity showed that cement design has more research gaps than others (Oil & Gas iQ, 2015). The study estimated that cement failure is one of the mainly reason to trigger well control loss (**Figure 2**).

Because geothermal well is one of the common component of high-temperature wells, the wellbore temperature is an important factor to induce the failure of the cement sheath. Based on the definition of NORSOR D-010 (2004), the temperature of high-temperature wells is typically above 150°C. Different from oil and gas wells, geothermal well does not generate any revenue until the nearby facilities such as power plant and electric grid have been constructed. Thus the long-term of integrity maintenance is significantly important for geothermal wells. High differential temperature in the system is a significant reason to induce cement failure (Okech et al. 2015). Expansion or shrinkage of cement caused by the difference of temperature between casing and reservoir can induce differential stress in the system and consequently trigger failure (Therond et al. 2016). Berndt and Philippacopoulos (2002) found that the cement with high tensile strength has the better sealability in geothermal wells. Compressive strength (Reddy et al. 2005) and porosity (Kuzielová et al. 2017) are variable with different curing temperatures. Moreover, cement-rock interactions are more active in the high temperature environment (Silva and Milestone 2018a and 2018b). Santoyo et al. (2001) and Song et al. (2019) tested thermal conductivity of six Mexican cementing systems and found empirical equations for correlating thermal conductivity with temperature of geothermal cement. Based on their experiments, thermal conduction decreases gradually with the rising temperature. In addition, Zhang and Wang (2017) used experiments to observed that thermal expansion in the cement sheath induced by expansion coefficient significant affects the wellbore integrity.

Not only thermal related properties, mechanical features are the other significant factors to contribute the failure of the cement sheath. Philippacopoulos and Berndt (2002) developed an analytical model to show that state of stress in the cement is sensitive to tectonic stresses and the relative stiffness between cement and formation. Hossain and Amro (2010) tested several cases and reported that differential pressure inducing from the difference between casing pressure and tectonic stresses increased the risk of cement failure. Nygaard et al. (2014) conducted a numerical simulation to study the effect of mechanical properties including Young's modulus and Poisson's ratio. Variable internal casing pressures and far-field tectonic stresses was applied as the boundary conditions. Based on the sensitivity analysis, high Young's modulus and high Poisson's ratio had benefits to maintain cement integrity (Also in agreement with Wu et al. 2020). In addition, the model also quantified that under the thermal cooling condition, it would be easier to induce the failure of debonding by decreasing the compressive mechanical stresses near the wellbore. Bios et al. (2011 and 2012) studied the effect of stiffness ratio of cement to formation on cement failure. The results showed that with decreasing temperature, the risk of casing-cement and cement-formation

debonding was high when formation was stiffer than cement. The risk of casing-cement interface debonding was more severe when cement coefficient of thermal dilation was small and cement was stiffer than formation. For a decreasing pore pressure environment, casing-cement and cement-formation bond failed when formation was stiffer than cement. Casing-cement debonding occurred when low cement Boit's coefficient was applied and cement was stiffer than formation.

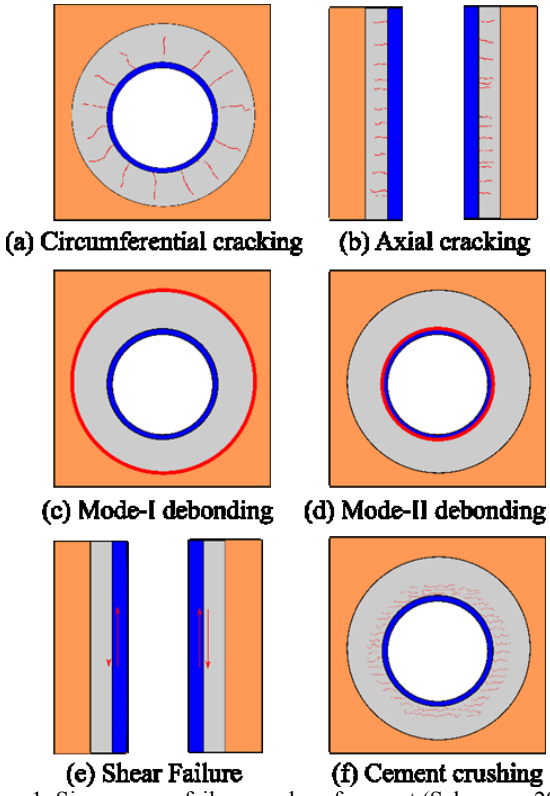

Figure 1: Six common failure modes of cement (Schrepper 2015)

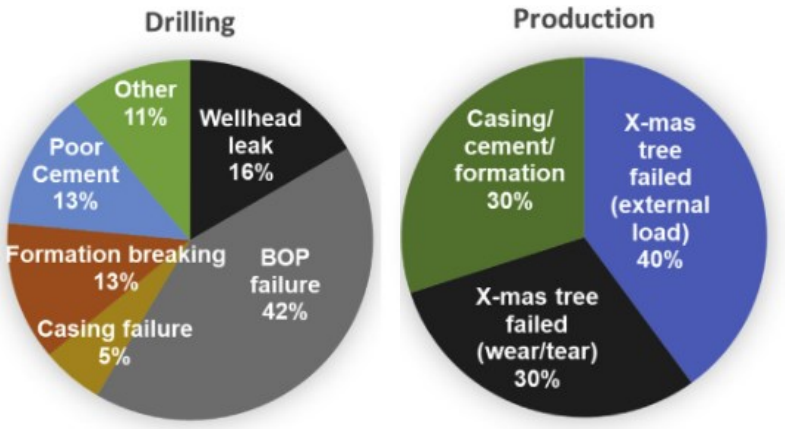

Figure 2: The reason of barrier failure during a) drilling operation and b) production in total 156 loss of well control events occurred between 2000 and 2015.

The geothermal wells are circulation system consisting both injection and production. Heat transfers from wellbore to reservoir in the production wells and in opposite direction in the injection wells. Although many previous researches have already studied the cement failure in heterogeneous temperature distribution, most of them are focused on one heat flow direction, either heat transfers from formation to casing or in opposite direction. The comparison of two differential temperature patterns was not understood. The specific objectives of this study were to: (i) compare the stress distribution in casing-cement-formation system under both differential temperature patterns or heat flow directions, (ii) assess influence of thermal parameters, other important material properties and operational factors that affect performance of cement. In this study, a verified 2D numerical model was created based on finite element analysis (FEA) method. The casing-cement sheath-formation system was simulated with two differential temperature modes, heat transfers from formation to casing (Ti < Tf) and opposite scenario (Ti > Tf). In each case, the failure location and likely mode were presented. Sensitivity response curves have been employed to rank and identify the influence of several parameters (i.e. thermal conductivity, expansion coefficient, differential temperature, internal casing pressure, Young's modulus, Poisson's ratio, and stress ratio).

2. METHODOLOGY

A two-dimension finite element model consisting of casing, cement, and formation was conducted in this study and the schematic is shown in **Figure 3**. The cement sheath with inner diameter (ID) of 7 inch (177.8 mm) and outer diameter (OD) of 8.75 inch (222.25 mm) was placed between casing and formation. Based on Jaeger et al. (2007), the dimension of formation was ten times of cement to decrease the boundary effect. Fine mesh was applied. The model was assumed as vertical wells. Tectonic stresses including maximum ($\sigma_{h\text{-}max}$) and minimum horizontal stresses ($\sigma_{h\text{-}min}$) were applied at the outer boundary of formation. Wellbore pressure (P_i) and temperature (T_i) were issued at the inner surface of casing. Reservoir temperature (T_f) was subjected to the outer boundary of the formation. θ was used to define the location. It was defined as the angle from maximum horizontal stress ($\sigma_{h\text{-}max}$). For example, θ equals 0° when the direction is parallel to $\sigma_{h\text{-}max}$ and 90° when perpendicular to the direction of $\sigma_{h\text{-}max}$ (**Figure 3**). The magnitude of boundary conditions such as tectonic stresses around the wellbore, casing pressure, and temperature are based on the Frontier Observatory for Research in Geothermal Energy (FORGE) geothermal wellbore in Utah shown in **Table 1**. The casing-cement and cement-formation surfaces were assumed to be bonded. Because according to experiment tests, cement is an extremely low permeability material (API states that the proper permeability of oil well cement should below 200μD) and the purpose of the study was to evaluate structural stresses. Hence, the cement sheath was modelled as a solid with linear elastic properties and treated as an impermeable material (Wu et al. 2020). The poroelastic effect was not considered in this study. **Table 2** shows the thermal and mechanical properties used in the base case.

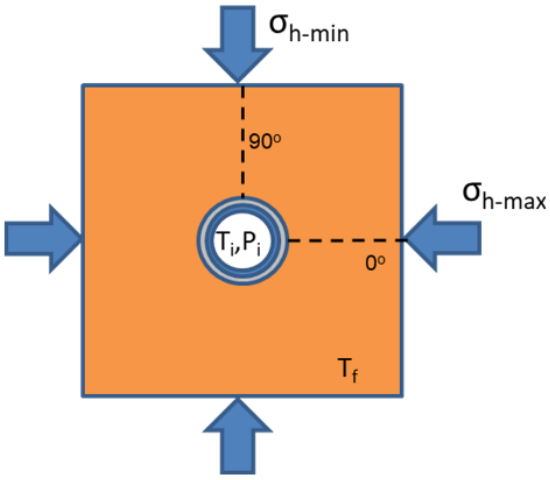

Figure 3: The schematic of the 2D numerical model with boundary conditions.

Table 1: The properties of FORGE geothermal wellbore (from Moore et al. 2019).

Depth	2300 m (7536 ft)
Maximum horizontal stress gradient	14.0 kPa/m (0.62 psi/ft)
Minimum horizontal stress gradient	17.4 kPa/m (0.77 psi/ft)
Bottom hole temperature	190°C (375°F)

Theoretically, annular cement sheath can be assumed as a thick- or thin-walled cylinder for calculating mechanical stresses under variable loadings. To evaluate the structural integrity of the cement sheath, cylindrical stresses in and around the wellbore were utilized. Cylinder stresses: radial and hoop stress are used to explain different failure modes in the cement sheath. Radial stress is the normal stress acting toward or away from the central axis of a cylinder. Hoop stress is defined as a normal stress in the tangential direction. In this study, the samples were tested in lab conditions. Therefore, in-situ stresses were not considered as a factor in failure criteria. The details of the failure criteria are shown in **Appendix A**.

Table 2: Material properties for the base case.

Model Component	*Parameter*	*Base Value*
Steel casing	Young's modulus, E_s (GPa)	200
	Poisson's ratio, ν_s	0.30
	Thermal expansion coefficient, α_s (10^{-6}/K)	11.43
	Thermal conductivity, K_s (W/m·K)	45
Cement sheath	Young's modulus, E (GPa)	12.5
	Poisson's ratio, ν	0.34
	Thermal expansion coefficient, α (10^{-6}/K)	9.4
	Thermal conductivity, K (W/m·K)	0.30
Formation	Young's modulus, E_f (GPa)	68.9
	Poisson's ratio, ν_f	0.26
	Thermal expansion coefficient, α_f (10^{-6}/K)	8.0
	Thermal conductivity, K_f (W/m·K)	2.90

**Cement and formation properties were cited from Kimanzi et al. 2019 and Moore et al. 2019 respectively.*

3. ANALYTICAL VERIFICATION

The analytical calculations were utilized for the verification of the numerical model (Li et al. 2010). Similar to FEA model, all interfacial connections were treated as bonded surfaces. The steel casing, cement sheath, and rock formation in the model were considered as thermos-linear elastic materials. There is no defect and the system is axisymmetric.

The model couples thermal and non-uniform in-situ stresses field together, it can be separated into two parts: the model imposed by (i) uniform inner and outer pressure with thermal effects and (ii) non-uniform outer pressure. The details of the derivation are shown in **Appendix B**. Because the derivation of radial (σ_r) and hoop (σ_θ) stresses has been published earlier (Li et al. 2010), in this study the procedure will not be repeated.

To complete the model verification, the internal casing temperature (T_i) and reservoir temperature (T_f) were selected to be 75°C and 190°C respectively. 10 MPa of casing pressure (P_i), 40 MPa of maximum horizontal stress ($\sigma_{h\text{-}max}$) and 32 MPa ($\sigma_{h\text{-}min}$) of minimum horizontal stress were applied in the model as boundary conditions. Two horizontal stresses were calculated based on the stress gradient of FORGE geothermal wellbore database as shown in **Table 1**. **Table 2** presented the details of material properties used in the validation. The casing, cement, and formation properties were all come from experiments and measurements (Kimanzi et al. 2019; Moore et al. 2019). Analytical results were calculated from the equations in **Appendix B** and compared with simulated radial and hoop stress in the cement sheath. The comparison is graphically presented in **Figure 4**. The results show that when casing temperature is less than formation ($T_i < T_f$), the deviation of FE simulation from analytical calculation is less than 7% (**Figure 3a** presents radial stress and **Figure 3b** presents hoop stress). When heat flows in an opposite direction, the deviation is less than 4% (**Figure 3c** presents radial stress and **Figure 3d** presents hoop stress). Based on the comparison, finite element model predictions match reasonably with the analytical calculations in both two heat flowing directions.

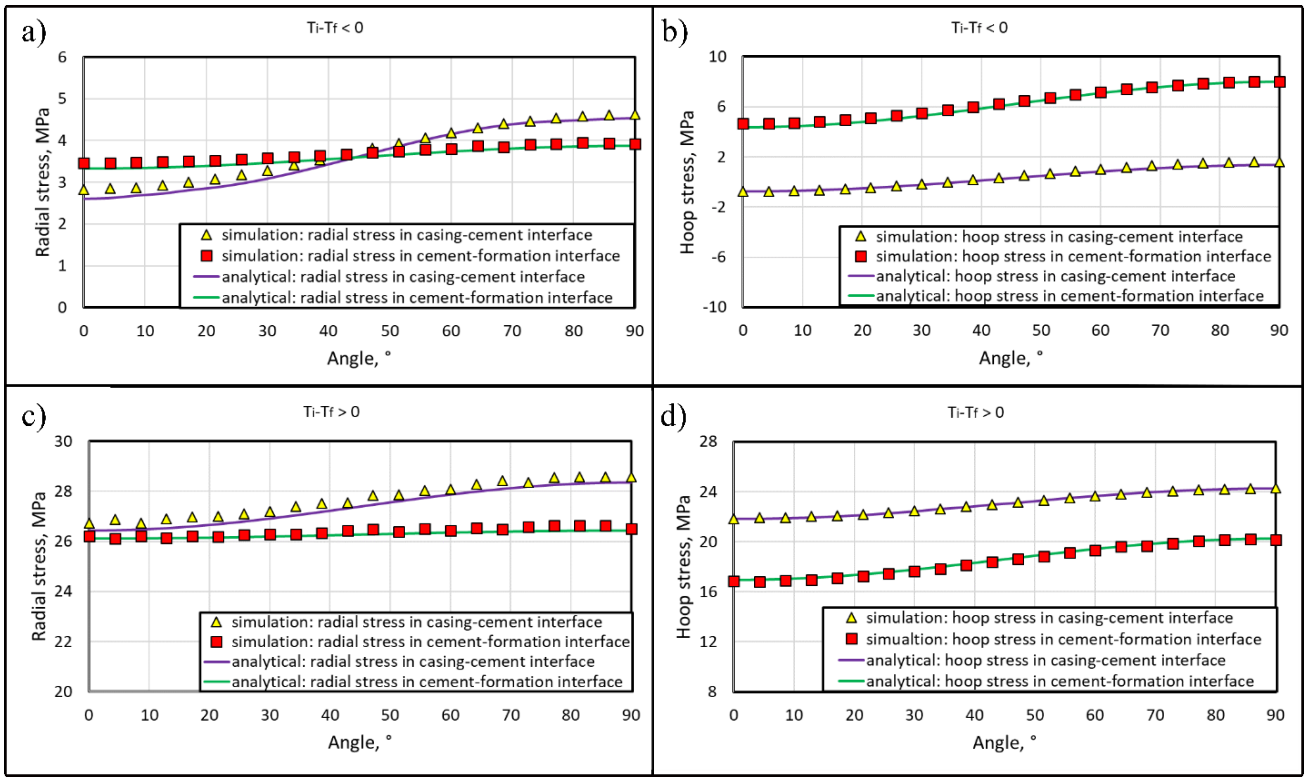

Figure 4: The comparison of radial and hoop stress at casing-cement and cement-formation interface between analytical and simulating results: a) radial and b) hoop stress distribution when heat flow toward casing; c) radial and b) hoop stress distribution eh heat flow away casing.

4. FAILURE ANALYSIS

In this section, two heat transferring patterns were tested. Three kinds of variables, thermal, mechanical, and operational properties, were tested individually in the study. By comparing these kinds of variables, the most affecting parameter could be found. **Table 3** is the list of variables investigated. The thermal properties involve thermal conductivity and expansion coefficient. Thermal conductivity represents the effect of temperature distribution on cement failure. Thermal expansion coefficient scales the thermal strain of material and the induced thermal stress if the thermal deformation is restraint (Zeng et al. 2012). Changing the coefficients results in different stress distribution and consequently different failure modes. The mechanical properties contain Young's modulus and Poisson's ratio. Internal casing pressure is one of the major load in a wellbore. The increment of the internal casing pressure happens during positive pressure tests, formation integrity tests, increased mud weight, and hydraulic fracture. The reduction of casing pressure occurs in the event of loss circulation or influx of lighter formation fluid (Patel and Salehi, 2019). Lithological properties are represented in terms of tectonic stress ratio (N_R). Tectonic stress ratio is mainly depended on lithology. It is defined as the ratio of maximum and minimum horizontal stress ($horizontal\ stress\ ratio = \frac{\sigma_{h-max}}{\sigma_{h-min}}$).

Table 3: The studied parameters for sensitivity response analysis

Parameter	*Base Value*	*Sensitivity Analysis Value*
Young's modulus (GPa)	12.5	5 (0.4), 10 (0.8), 12.5 (1.0), 20 (1.6), 35 (2.8)
Poisson's ratio	0.34	0.20 (0.59), 0.25 (0.74), 0.34 (1.0), 0.45 (1.32)
Horizontal stress ratio	1.25	1.00 (0.80), 1.25 (1.0), 2.00 (1.60), 2.50 (2.0)
Thermal conductivity of cement (W/m•K)	0.3	0.2 (0.67), 0.3 (1.0), 0.5 (1.67), 1.0 (3.33)
Expansion coefficient of cement (10^{-6}/K)	9.4	7.0 (0.74), 8.0 (0.85), 9.4 (1.0), 11.0 (1.17), 12.0 (1.28)
Differential temperature (|°C|)	115	0 (0), 40 (0.35), 65 (0.57), 90 (0.78), 115 (1.0), 140 (1.22)
Casing pressure (MPa)	10	0 (0), 5 (0.5), 10 (1.0), 15 (1.5), 20 (2)

** The temperature difference (ΔT) for conductivity, expansion coefficient, Young's modulus, Poisson's ratio, stress ratio and casing pressure cases is 115°C.*

*** Numbers inside parenthesis are normalized values of parameters.*

The sensitivity response curve was used to compare the impact of different parameters on the cylindrical stresses in a single plot. The analysis ignored the effect of temperature on the material properties. Each variable was changed individually while keeping the other variables constant. To make the properties comparable, the normalized parameter value was used (Patel and Salehi 2019). It is calculated by dividing the value of parameter in each case by the base case value ($normalized\ parameter = \frac{parameter\ value}{base\ case\ value}$). The sensitivity response curves are expressed by the relationship between the outcome values (radial and hoop stress) and normalized parameters. Radial and hoop stress along cement thickness at 0° and 90° directions for different temperatures have been illustrated in **Appendix C**. The results show that the highest magnitude of stresses and consequently high risk of integrity loss is at the cement-casing interface of the cement sheath. Authors has also tested the cases with the other variates (Young's modulus, Poisson's ratio, thermal conductivity, expansion coefficient, temperature, and casing pressure). All cases in agreement with the same regularity as shown in **Appendix C**. Therefore, in order to simplify the comparison, sensitivity response analysis is only presented at the casing-cement interface.

4.1. Heat Flow from Formation to Casing (ΔT < 0)

Heat flow transferring from formation to casing is representative of injection wells. Especially in the geothermal wellbore, cold fluid is injected to the high temperature reservoir, with increasing depth, the temperature difference tends to higher than shallow depth. **Figure 5** and **Figure 6** illustrate the cylindrical stresses in the casing-cement interface at both 0° and 90° when ΔT < 0.

4.1.1. Radial stress

For the radial stresses in 0° and 90° (**Figure 5**), differential temperature is the most sensitive parameter followed by internal casing pressure and horizontal stress ratio (**Table 3**). The other parameters such as thermal conductivity, expansion coefficient, Young's modulus and Poisson's ratio do not exert notable influence on the radial stress. Increase in casing pressure increases the compressive nature and magnitude of radial stress. On the other hand, increase in differential temperature and horizontal stress ratio reduces radial stress and make them more tensile. The tensile stress at 0° (**Figure 5a**) is larger than at 90° (**Figure 5b**).

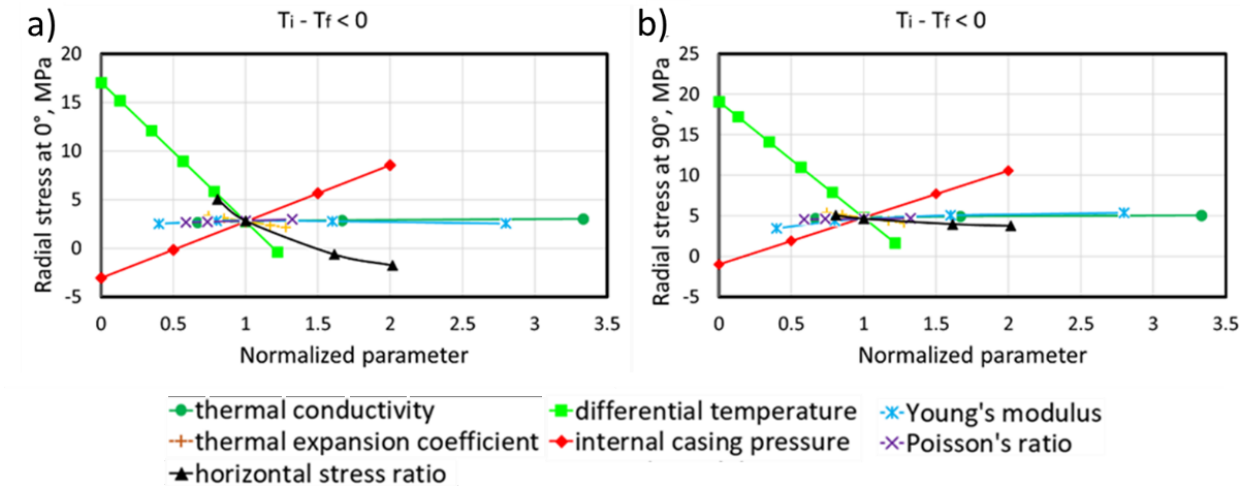

Figure 5: Radial stress in the casing-cement interface when heat transfers from formation to casing (ΔT < 0) a) at 0° and b) at 90°.

4.1.2. Hoop stress

For the hoop stresses (**Figure 6**), thermal expansion coefficient is the most critical parameter followed by differential temperature, horizontal stress ratio, and Young's modulus (**Table 3**). Increase in temperature difference, horizontal stress ratio, and thermal expansion coefficient tend to reduce the hoop stress and make it more tensile. In general, hoop stress at 90° direction has higher magnitude than along 0°.

The comparison shows that the debonding and radial fracture at casing-cement interface in 0° is the most possible failure mode. For both cylindrical stresses (radial and hoop), differential temperature, and horizontal in-situ stress are the critical parameters. For hoop stress, thermal expansion coefficient is also highly influential variable.

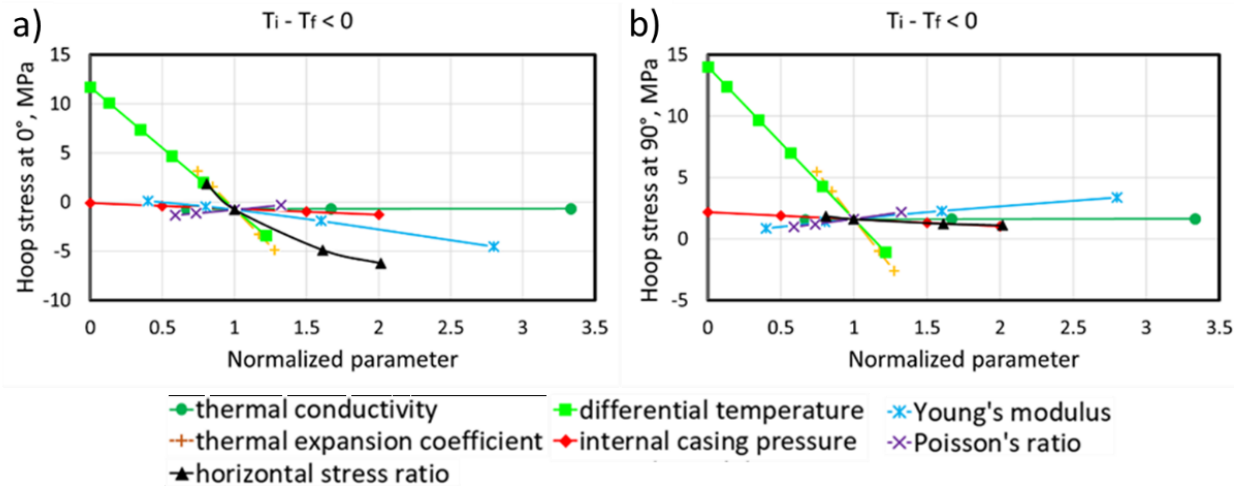

Figure 6: Hoop stress in the casing-cement interface when heat transfers from formation to casing ($\Delta T < 0$) a) at 0° and b) at 90°.

4.2. Heat Flow from Casing to Formation ($\Delta T > 0$)

Casing temperature larger than formation temperature is a likely scenario in production wells wherein high temperature geothermal fluid is produced. Especially against shallow depth, where the temperature of rock formation is relatively low. **Figure 7** and **Figure 8** illustrate the cylindrical stress in the casing-cement interface at both 0° and 90° when $\Delta T > 0$. The stresses are predominantly compressive.

4.2.1. Radial stress

For the radial stress (**Figure 7**), the effect of the variates in parallel and perpendicular directions are similar. The magnitudes of compression in perpendicular direction (i.e. 90°) are larger than parallel (i.e. 0°). The most sensitive parameter to the radial stress is the differential temperature followed by internal casing pressure, Young's modulus, and stress ratio (details are shown in **Table 4**). Young's modulus and stress ratio are more sensitive at low magnitudes compared to higher magnitudes. High differential temperature, casing pressure, Young's modulus and low stress ratio results in sufficient compressive stress to exceed the limitation of cement strength. It would increase the risk of cement crushing.

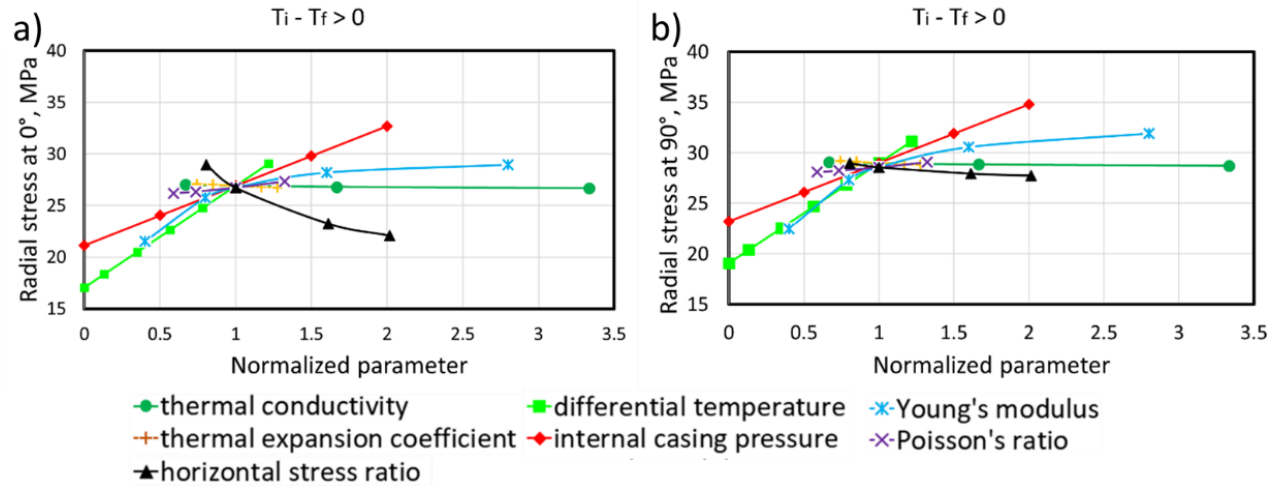

Figure 7: Radial stress in the casing-cement interface when heat transfers from casing to formation ($\Delta T > 0$) a) at 0° and b) at 90°.

4.2.2. Hoop stress

For the hoop stress (**Figure 8**), stress has the largest sensitivity to change in Young's modulus. The other parameters, such as Poisson's ratio, differential temperature, and stress ratio also induce notable change (details are shown in **Table 4**). Same as radial stress, the compressive stress in perpendicular direction is slightly larger than parallel. Increasing Young's modulus, differential temperature, and Poisson's ratio result in higher compressive hoop stress. Contrary to this, increase in stress ratio reduces compressive nature of hoop stress and pushes it towards tensile.

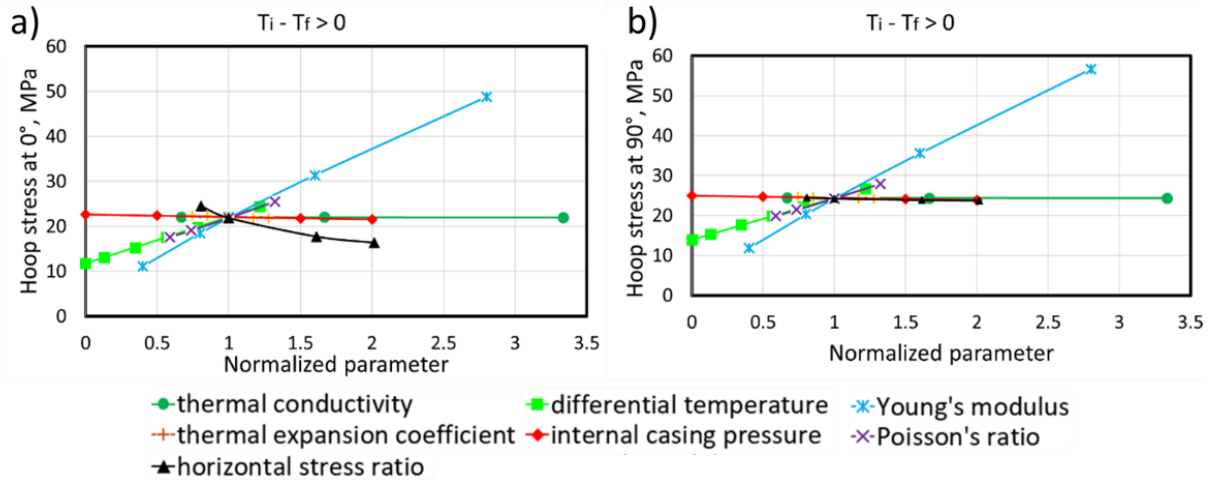

Figure 8: Hoop stress in the casing-cement interface when heat transfers from casing to formation (ΔT > 0) a) at 0° and b) at 90°.

Table 4: The comparison of mechanical stresses sensitivity to various parameters.

Direction	*Radial stress (σ_r)*	*Hoop stress (σ_θ)*
	ΔT < 0	
0°	$\Delta T > Pi > N_R$ (α, K, E, and ν are not sensitive)	$\alpha > \Delta T > N_R > E$ (K, ν, and Pi are not sensitive)
90°	$\Delta T > Pi > N_R$ (α, K, E, and ν are not sensitive)	$\alpha > \Delta T > N_R > E$ (K, ν, and Pi are not sensitive)
	ΔT > 0	
0°	$\Delta T > Pi > E > N_R$ (K, α, and ν are not sensitive)	$E > \nu > \Delta T > N_R$ (K, Pi, and α are not sensitive)
90°	$\Delta T > Pi > E > N_R$ (K, α, and ν are not sensitive)	$E > \nu > \Delta T > N_R$ (K, Pi, and α are not sensitive)

The comparison of two directions under the condition of ΔT > 0 shows that the cement crushing (compressive failure) in the casing-cement interface at 90° is the most likely failure mode compared to the tensile failures.

5. CONCLUSION

This study investigates integrity of cement bonded between casing and formation under the influence of thermal stresses. An analytical model is used to generate theoretical values of stresses to verify 2D finite element model of the casing-cement-formation system. Finite element simulations show a good match with analytical model of radial and hoop stress. The deviation between FEA and analytical calculations for both heat flow directions (ΔT > 0 and ΔT < 0) is less than 7%. Various scenarios are simulated to study the influence of temperature difference, thermal conductivity, and thermal expansion coefficients, on stresses in cement. Sensitivity analysis has been presented to show the influence of thermal factors relative to other important parameters like casing pressure, cement material properties, and in-situ geo-mechanical stresses. Following points are concluded from the study that help improve understanding of cement failure:

- When heat transfer from casing to formation (ΔT > 0) with large temperature difference, the risk of cement crushing near casing-cement interface at 90° is high. When heat transfer in the opposite direction, radial fracture near casing-cement interface at 0° is the likely failure model.
- Stress distributions in wellbore were investigated for various simulation cases. It was observed that magnitude of radial and hoop stress and consequently the risk of failure is higher at the cement-casing interface compared to other locations within wellbore. Along casing-cement interface, risk of failure is high in directions parallel (0°) and perpendicular (90°) to maximum horizontal in-situ stress.
- For the range of parameters investigated, scenarios with heat transfer away from the wellbore exhibited higher magnitude of stresses than cases with heat transfer towards wellbore.
- Sensitivity analysis indicates that regardless of the direction of heat transfer, radial and hoop stress in cement have higher sensitivity to temperature changes compared to pressure load.
- Regardless of direction of heat transfer, radial stress in cement has high sensitivity to both temperature difference, and pressure load. Thermal conductivity and expansion coefficient has no significant influences.
- For hoop stress, temperature difference has high impact but pressure load does not have high influence while for radial stress

both two parameters are significant to evaluate cement failure. Thermal conductivity is not important and thermal expansion coefficient is influential only for heat transfer direction towards wellbore.

ACKNOWLEDGEMENTS

Authors of this paper would like to thank U.S. Department of Energy's Office of Energy Efficiency and Renewable Energy (EERE) under the Geothermal Program Office Award Number DE-EE0008602 for providing travel support to attend 45th Workshop on Geothermal Reservoir and present this work.

NOMENCLATURE

Acronyms:

API	American Petroleum Institute
FEA	Finite element analysis
FORGE	Frontier Observatory for Research in Geothermal Energy
ID	Inner diameter
OD	Outer diameter

Symbols:

a	Inner diameter of casing
b	Outer diameter of casing
c	Inner diameter of formation
d	outer diameter of formation
r	Radial distance from the center of the wellbore
p_2	Casing-cement interfacial pressure
p_3	Cement-formation interfacial pressure
u_{rc}, u_r, u_{rf}	Total radial displacement in casing, cement, and formation respectively
u_{pc}, u_p, u_{pf}	Radial displacement induced by uniform pressure in casing, cement, and formation respectively
u_{Tc}, u_T, u_{Tf}	Radial displacement induced by temperature in casing, cement, and formation respectively
σ_{rc}, σ_r, σ_{rf}	Radial stresses in casing, cement, and formation respectively
τ_{rc}, τ_r, τ_{rf}	Shear stresses in casing, cement, and formation respectively
J, M, K	Constant to calculate radial, hoop, and shear stress under non-uniform formation pressure
p_f'	Non-uniform pressure of the formation
T_i	Casing temperature
T_f	Formation temperature
ΔT	Differential temperature between casing and formation
P_i	Casing pressure
N_R	Tectonic stress ratio
$\sigma_{h\text{-}max}$	Maximum horizontal stress
$\sigma_{h\text{-}min}$	Minimum horizontal stress
θ	Angle to the maximum horizontal stress
σ_θ	Hoop stress
σ_r	Radial stress
T_o	Tensile strength of the cement sheath
C_o	Compressive strength of the cement sheath
E_s, E, E_f	Young's modulus of casing, cement, and formation respectively
ν_s, ν, ν_f	Poisson's ratio of casing, cement, and formation respectively
α_s, α, α_f	Thermal expansion coefficient of casing, cement, and formation respectively
K_s, K, K_f	Thermal conductivity of casing, cement, and formation respectively

REFERENCES

Berndt, M.L. and Philippacopoulos, A.J.: Incorporation of Fibres in Geothermal Well Cements, *Geothermics*, **31**, (2002), 643-656.

Bustgaard, M. and Nesheim, M.H.: Model for Prediction of Cement Sheath Failure, *M.S. thesis*. Norwegian University of Science and Technology, (2016).

Bois, A.P., Garnier, A., Rodot, F., Sain-Marc, J., and Aimard, N.: How to Prevent Loss of Zonal Isolation Through a Comprehensive Analysis of Microannulus Formation, *SPE Drilling & Completion*, **26**, (2011), 13-31.

Bois, A.P., Garnier, A., Galdiolo, G., and Laudet, J.B.: Use of a Mechanistic Model to Forecast Cement Sheath Integrity, *SPE Drilling & Completion*, **27**, (2012), 303-314.

Davies, R.J., Almond, S., Ward, R.S., Jackson, R.B., Adams, C., Worrall, F., Herringshaw, L.G., Gluyas, J.G., and Whitehead, M.A.: Oil and Gas Wells and Their Integrity: Implications for Shale and Unconventional Resource Exploitation, *Marine and Petroleum Geology*, **56**, (2014), 239-254.

De Andrade, J. and Sangesland, S.: Cement Sheath Failure Mechanisms: Numerical Estimates to Design for Long-Term Well Integrity, *Journal of Petroleum Science and Engineering*, **147**, (2016), 682-698.

Garnier, A., Saint-Marc, J., Bois, A.P., and Kermanac'h, Y.: An Innovative Methodology for Designing Cement-Sheath Integrity Exposed to Steam Stimulation, *SPE Drilling and & Completion*, **25**, (2010), 58-69.

Hossain, M.M. and Amro, M.: Drilling and Completion Challenges and Remedies of CO2 Injected Wells with Emphasis to Mitigate Well Integrity Issues, SPE Asia Pacific Oil and Gas Conference and Exhibition, 18-20 October, Brisbane, Queensland, Australia, (2010).

Jaeger, J.C., Cook, N.G.W., and Zimmerman, R.W.: Fundamentals of Rock Mechanics, 4th edition. Malden, MA: Blackwell Pub., (2007).

Kimanzi, R., Patel, H., Khalifeh, M., Salehi, S., and Teodoriu, C.: Potentials of Nano-Designed Plugs: Implications for Short and Long

Term Well Integrity, ASME 2019 38th International Conference on Ocean, Offshore and Arctic Engineering, June 9–14, 2019, Glasgow, Scotland, UK, (2019).

Kiran, R., Teodoriu, C., Dadmohammadi, Y., Nygaard, R., Wood, D., Mokhtari, M. and Salehi, S.: Identification and Evaluation of Well Integrity and Causes of Failure of Well Integrity Barriers (A Review), *Journal of Nature Gas Science and Engineering*, **45**, (2017), 511-526.

Kuzielová, E., Žemlička, M., Másilko, J., and Palou, M.T.: Pore Structure Development of Blended G-Oil Well Cement Submitted to Hydrothermal Curing Conditions, *Geothermics*, **68**, (2017), 86-93.

Lavrov, A. and Torsæter, M.: Physics and Mechanics of Primary Well Cementing, 1st ed., Springer, New York, (2016).

Li, Y., Liu, S., Wang, Z., Yuan, J., and Qi, F.: Analysis of Cement Sheath Coupling Effects of Temperature and Pressure in Non-Uniform In-Situ Stress Field, International Oil and Gas Conference and Exhibition in China, 8-10 June, Beijing, China, (2010).

Moore, J., McLennan, J., Allis, R., Pankow, K., Simmons, S., Podgorney, R., Wannamaker, P., Bartley, J., Jones, C., and Rickard, W.: The Utah Frontier Observatory for Research in Geothermal Energy (FORGE): An International Laboratory for Enhanced Geothermal System Technology Development, 44th Workshop on Geothermal Reservoir Engineering, 11-13 February, Stanford, California, (2019).

NORSOK D-010: Well Integrity in Drilling and Well Operations, 4th edition, Lysaker, Norway: Standards Norway, (2013).

Nygaard, R., Salehi, S., Weideman, B., and Lavoie, R.G.: Effect of Dynamic Loading on Wellbore Leakage for the Wabamun Area CO2 Sequestration Project, *Journal of Canadian Petroleum Technology*, **53**, (2014), 69-82.

Okech, R.R., Liu, X., Falcone, G., and Teodoriu, C.: Unconventional Completion Design for Deep Geothermal Wells, SPE Latin American and Caribbean Petroleum Engineering Conference, 18-20 November, Quito, Ecuador, (2015).

Oil & Gas iQ: High Pressure High Temperate, High Costs, High Stakes? https://www.oilandgasiq.com/content-auto-download/5b04c1b543dfd0385d3c7c22. (Accessed Oct. 4, 2018).

Patel, H. and Salehi, S.: Development of an Advanced Finite Element Model and Parametric Study to Evaluate Cement Sheath Barrier, *Journal of Energy Resource Technology*, **141**, (2019).

Patel, H., Salehi, S., and Teodoriu, C.: Assessing Mechanical Integrity of Expanding Cement, SPE Oklahoma City Oil and Gas Symposium, 9-10 April, Oklahoma City, Oklahoma, USA, (2019).

Philippacopoulos, A.J. and Berndt, M.L.: Structural Analysis of Geothermal Well Cements, *Geothermics*, **31**, (2002), 657-676.

Reddy, B.R., Santra, A.K., McMechan, D.E., Gray, D.W., Brenneis, C., and Dunn, R.: Cement Mechanical Property Measurements Under Wellbore Conditions, SPE Annual Technical Conference and Exhibition, 9-12 October, Dallas, Texas, USA, (2005).

Santoyo, E., García, A., Morales, J.M., Contreras, E., and Espinosa-Paredes, G.: Effective Thermal Conductivity of Mexican Geothermal Cementing Systems in The Temperature Range from 28°C to 200°C, *Applied Thermal Engineering*, **21**, (2001), 1799-1812.

Schreppers, G.: A Framework for Wellbore Cement Integrity Analysis, 49th U.S. Rock Mechanics/Geomechanics Symposium, 28 June-1 July, San Francisco, California, USA, (2015).

Silva, J.C. and Milestone, N.B.: The Effect of the Rock Type On the Degradation of Well Cements in CO_2 Enriched Geothermal Environments, *Geothermics*, **75**, (2018a), 235-248.

Silva, J.C. and Milestone, N.B.: Cement/Rock Interaction in Geothermal Wells. The Effect of Silica Addition to The Cement and The Impact of CO_2 Enriched Brine, *Geothermics*, **73**, (2018b), 16-31.

Song, X., Rui, Z., Ruixia, L., Gensheng, L., Baojiang, S., Yu, S., Gaosheng, W., and Shijie, Z.: Study On Thermal Conductivity of Cement with Thermal Conductive Materials in Geothermal Well, *Geothermics*, **81**, (2019), 1-11.

Therond, E., Bois, A.P., Whaley, K., and Murillo, R.: Large Scale Testing & Modelling for Cement Zonal Isolation of Water Injection Wells, SPE Annual Technical Conference and Exhibition, 26-28 September, Dubai, UAE, (2016).

Wang, W. and Taleghani, A.D.: Three-Dimensional Analysis of Cement Sheath Integrity Around Wellbores, *Journal of Petroleum Engineering*, **121**, (2014), 38-51.

Wise, J., Nygaard, R., and Hareland, G.: Numerical Analysis of Wellbore Integrity and Cement Sheath Debonding for Wells in the Eugene Island OPD, Gulf of Mexico, 53rd U.S. Rock Mechanics/Geomechanics Symposium, 23-26 June, New York City, New York, (2019).

Wu, Y., Patel, H., Salehi, S., and Mokhtari, M.: Experimental and finite element modelling evaluation of cement integrity under diametric compression, *Journal of Petroleum Science and Engineering*, **188**, (2020).

Zhang, Z. and Wang, H.: Effect of Thermal Expansion Annulus Pressure On Cement Sheath Mechanical Integrity in HPHT Gas Wells, *Applied Thermal Engineering*, **118**, (2017), 600-611.

APPENDIX A: FAILURE CRITERIA

Based on Schrepper (2015), ignoring the in-situ stresses, radial cracking develops when the hoop stress exceeds the tensile strength of cement sheath (Garnier et al. 2010, Bustgaard and Nesheim 2016, Patel et al. 2019). Compressive failure initiates when the hoop stress exceeds the compressive strength of cement (Lavrov and Torsæter 2016):

$$\text{Circumferential cracking: } \sigma_\theta \geq T_o \text{ (tension)} \quad \text{(A1)}$$

$$\text{Cement crushing: } |\sigma_\theta| \geq C_o \text{ (compression)} \quad \text{(A2)}$$

Where σ_θ is the hoop stress. T_o and C_o are the tensile and compressive strength of the cement sheath, respectively.

Debonding initiates when radial stress at casing-cement or cement-formation interface exceeds the tensile strength of the cement (Lavrov and Torsæter 2016). When radial stress is compressive and the magnitude exceeds the compressive strength of the cement, stress crushing occurs (Lavrov and Torsaeter 2016).

$$\text{Radial debonding (mode-I and mode-II debonding): } \sigma_r \geq T_o \text{ (tension)} \quad \text{(A3)}$$

$$\text{Cement crushing: } |\sigma_r| \geq C_o \text{ (compression)} \quad \text{(A4)}$$

Where σ_r is the radial stress. It is important to note that although the compressive strength is more than 10 times of tensile strength in the cement sheath (De Andrade and Sangesland 2016), the compressive mode of failure is still needed to be evaluated because of potential compressive loads.

APPENDIX B: THE DERIVATION OF THE ANALYTICAL MODEL

In this section, the details of the stress in casing-cement-formation system are shown. The non-uniform in-situ stresses field is separated into two parts, (i) uniform inner and outer pressure with thermal effects and (ii) non-uniform outer pressure. For situation (i), because of the differential temperature between casing (T_i) and reservoir (T_f) the temperature distribution within the cement along the radial orientation (T) is:

$$T = T_i - (T_i - T_f)\frac{ln\frac{r}{b}}{ln\frac{c}{b}} \tag{B1}$$

The radial (ε_r), hoop (ε_θ), and axial (ε_z) strain can be written as:

$$\begin{cases} \varepsilon_r = \frac{1}{E}[\sigma_r - v(\sigma_\theta + \sigma_z)] + \alpha T \\ \varepsilon_\theta = \frac{1}{E}[\sigma_\theta - v(\sigma_z + \sigma_r)] + \alpha T \\ \varepsilon_z = \frac{1}{E}[\sigma_z - v(\sigma_r + \sigma_\theta)] + \alpha T \end{cases} \tag{B2}$$

Where E is Young's modulus, ν is Poisson's ratio, and α is thermal expansion coefficient. Because plane strain theory is applied in the model, ε_z is zero.

$$\sigma_z = v(\sigma_r + \sigma_\theta) - E\alpha T \tag{B3}$$

Combine Equation B3 with Equation B2:

$$\begin{cases} \varepsilon_r = \frac{1+v}{E}[(1-v)\sigma_r - v\sigma_\theta] + (1+v)\alpha T \\ \varepsilon_\theta = \frac{1+v}{E}[(1-v)\sigma_\theta - v\sigma_r] + (1+v)\alpha T \end{cases} \tag{B4}$$

Then re-write Equation B4 in to Equation B5:

$$\begin{cases} \sigma_r = \frac{E}{(1+v)(1-2v)}[(1-v)\varepsilon_r + v\varepsilon_\theta - (1+v)\alpha T \\ \sigma_\theta = \frac{E}{(1+v)(1-2v)}[(1-v)\varepsilon_\theta + v\varepsilon_r - (1+v)\alpha T \end{cases} \tag{B5}$$

Radial and hoop stress need to satisfy the balance equation (Equation B6):

$$\frac{d\sigma_r}{dr} + \frac{\sigma_r - \sigma_\theta}{r} = 0 \tag{B6}$$

Combine Equation B4 and B6 together, the displacement (u) can be calculated by:

$$\frac{d}{dr}\left[\frac{1}{r}\frac{d(ru)}{dr}\right] = \alpha\frac{1+v}{1-v}\frac{dT}{dr} \tag{B7}$$

Because of the strain-displacement relationship (Equation B8), strains can be written as:

$$\begin{cases} \varepsilon_r = \frac{du}{dr} = \alpha\frac{1+v}{1-v}(T - \frac{1}{r^2}\int_{r_i}^{r} Trdr) + R_1 - \frac{R_2}{r^2} \\ \varepsilon_\theta = \frac{u}{r} = \alpha\frac{1+v}{1-v}\frac{1}{r^2}\int_{r_i}^{r} Trdr + R_1 + \frac{R_2}{r^2} \end{cases} \tag{B8}$$

According to Equation B5, Equation B8 can be written as:

$$\begin{cases} \sigma_r = \frac{E}{1+v}[-\alpha\frac{1+v}{1-v}\frac{1}{r^2}\int_{r_i}^{r} Trdr + \frac{R_1}{1-2v} - \frac{R_2}{r^2} \\ \sigma_\theta = \frac{E}{1+v}[\alpha\frac{1+v}{1-v}\frac{1}{r^2}\int_{r_i}^{r} Trdr + \frac{R_1}{1-2v} + \frac{R_2}{r^2} - \alpha\frac{1+v}{1-v}T \end{cases} \tag{B9}$$

In Equation B8 and B9, R_1 and R_2 are the integral constant. p_2 and p_3 are determined by the displacement boundary conditions (Equation A10).

$$\begin{cases} u_{rc}|_{r=b} = u_{pc}|_{r=b} + u_{Tc}|_{r=b} \\ u_r|_{r=b} = u_p|_{r=b} + u_T|_{r=b} \\ u_r|_{r=c} = u_p|_{r=c} + u_T|_{r=c} \\ u_{rf}|_{r=c} = u_{pf}|_{r=c} + u_{Tf}|_{r=c} \end{cases} \tag{B10}$$

The cylindrical stresses near the wellbore in the casing-cement-formation system can be estimated using the following equations (Equation B11):

$$\begin{cases}\sigma_r = \frac{b^2 p_2 - c^2 p_3}{c^2 - b^2} - \frac{b^2 c^2 (p_2 - p_3)}{c^2 - b^2}\frac{1}{r^2} \\ \sigma_\theta = \frac{b^2 p_2 - c^2 p_3}{c^2 - b^2} + \frac{b^2 c^2 (p_2 - p_3)}{c^2 - b^2}\frac{1}{r^2}\end{cases}$$

(B11)

For situation (ii), the stress induced by non-uniform pressure is analyzed. The Airy stress function (φ) is related to the stress tensor (σ) by:

$$\begin{cases}\sigma_r = \frac{1}{r}\frac{\partial \varphi}{\partial r} + \frac{1}{r^2}\frac{\partial^2 \varphi}{\partial \theta^2} \\ \sigma_\theta = \frac{\partial^2 \varphi}{\partial r^2} \\ \tau_{r\theta} = -\frac{\partial}{\partial r}\left(\frac{1}{r}\frac{\partial \varphi}{\partial \theta}\right)\end{cases}$$

(B12)

The Airy stress function can be assumed as:

$$\varphi = \left(Jr^2 + Kr^4 + \frac{M}{r^2} + N\right) cos2\theta$$

(B13)

Where J, K, M, and N are the unknown constants and required to be determined. The stresses can be expressed by Equation B12 and B13:

$$\begin{cases}\sigma_r = -2\left(J + \frac{3M}{r^4} + \frac{2N}{r^2}\right) cos2\theta \\ \sigma_\theta = 2\left(J + 6Kr^2 + \frac{3M}{r^4}\right) cos2\theta \\ \tau_{r\theta} = 2\left(J + 3Kr^2 - \frac{3M}{r^4} - \frac{N}{r^2}\right) sin2\theta\end{cases}$$

(B14)

The strains are determined by:

$$\begin{cases}\varepsilon_r = \frac{1-v^2}{E}\left(\sigma_r - \frac{v}{1-v}\sigma_\theta\right) \\ \varepsilon_\theta = \frac{1-v^2}{E}\left(\sigma_\theta - \frac{v}{1-v}\sigma_r\right) \\ \varepsilon_{r\theta} = \frac{1+v}{E}\tau_{r\theta}\end{cases}$$

(B15)

Combine Equation B14 and B15 together:

$$\begin{cases}\varepsilon_r = -\frac{2(1+v)}{E}\left[J + 6Kr^2 v + \frac{3M}{r^4} + \frac{2N}{r^2}(1-v)\right] cos2\theta \\ \varepsilon_\theta = \frac{2(1+v)}{E}\left[J + 6(1-v)Kr^2 + \frac{3M}{r^4} + \frac{2N}{r^2}v\right] cos2\theta \\ \varepsilon_{r\theta} = \frac{2(1+v)}{E}\left(J + 3Kr^2 - \frac{3M}{r^4} - \frac{N}{r^2}\right) sin2\theta\end{cases}$$

(B16)

Because of the geometric equation, $\varepsilon_r = \frac{du}{dr}$ and $\varepsilon_\theta = \frac{u}{r}$, Equation B16 can be written as:

$$\begin{cases}\varepsilon_r = \frac{\partial u_r}{\partial r} \\ \varepsilon_\theta = \frac{1}{r}\frac{\partial u_\theta}{\partial \theta} + \frac{u_\theta}{r} \\ \varepsilon_{r\theta} = \frac{1}{2}\left[\frac{1}{r}\frac{\partial u_r}{\partial \theta} + \frac{\partial u_\theta}{\partial r} - \frac{u_\theta}{r}\right]\end{cases}$$

(B17)

So the radial and hoop displacements is derived by the Equation B18:

$$\begin{cases}u_r = -\frac{2(1+v)}{E}\left[Jr + 2Kr^3 v - \frac{M}{r^3} - \frac{2N}{r}(1-v)\right] cos2\theta + f(\theta) \\ u_\theta = \frac{2(1+v)}{E}\left[Jr + (3-2v)Kr^3 + \frac{M}{r^3} + \frac{N}{r}(2v-1)\right] sin2\theta - \int f(\theta)d\theta + g(r)\end{cases}$$

(B18)

$f(\theta)$ and $g(r)$ are neglected because the formulations calculate the rigid body displacements which is not considered in this study. So the Equation B18 is:

$$\begin{cases} u_r = -\frac{2(1+v)}{E}\left[Jr + 2Kr^3v - \frac{M}{r^3} - \frac{2N}{r}(1-v)\right]cos2\theta \\ u_\theta = \frac{2(1+v)}{E}\left[Jr + (3-2v)Kr^3 + \frac{M}{r^3} + \frac{N}{r}(2v-1)\right]sin2\theta \end{cases}$$

(B19)

Based on the boundary conditions in Equation B20, 12 equations (Equation B21) are generated to solve J_c, K_c, M_c, N_c, J, K, M, N, J_f, K_f, M_f, and N_f:

$$\begin{cases} \sigma_{rc} = 0, \tau_{r\theta c} = 0 \\ \sigma_{rc} = \sigma_r, \tau_{r\theta c} = \tau_{r\theta} \\ u_{rc} = u_r, u_{\theta c} = u_\theta \\ \sigma_{rf} = \sigma_r, \tau_{r\theta f} = \tau_{r\theta} \\ u_{rf} = u_r, u_{\theta f} = u_\theta \\ \sigma_{rf} = -p_f', \tau_{r\theta f} = \tau_f \end{cases}$$

(B20)

$$\begin{cases} J_c + \frac{3M_c}{a^4} + \frac{2N_c}{a^2} = 0 \\ J_c + 3K_c a^2 - \frac{3M_c}{a^4} - \frac{N_c}{a^2} = 0 \\ J_c + \frac{3M_c}{b^4} + \frac{2N_c}{b^2} = J + \frac{3M}{b^4} + \frac{2N}{b^2} \\ J_c + 3K_c b^2 - \frac{3M_c}{b^4} - \frac{N_c}{b^2} = J + 3Kb^2 - \frac{3M}{b^4} - \frac{N}{b^2} \\ J_c b + 2K_c b^3 v_c - \frac{M_c}{b^3} - \frac{2N_c}{b}(1-v_c) = \frac{E_c(1+v)}{E(1+v_c)}[Jb + 2Kb^3 v - \frac{M}{b^3} - \frac{2N}{b}(1-v)] \\ J_c b + (3-2v_c)K_c b^3 + \frac{M_c}{b^3} + \frac{N_c}{b}(2v_c - 1) = \frac{E_c(1+v)}{E(1+v_c)}[Jb + (3-2v)Kb^3 + \frac{M}{b^3} + \frac{N}{b}(2v-1)] \\ J_f + \frac{3M_f}{c^4} + \frac{2N_f}{c^2} = J + \frac{3M}{c^4} + \frac{2N}{c^2} \\ J_f + 3K_f c^2 - \frac{3M_f}{c^4} - \frac{N_f}{c^2} = J + 3Kc^2 - \frac{3M}{c^4} - \frac{N}{c^2} \\ J_f c + 2K_f c^3 v_f - \frac{M_f}{c^3} - \frac{2N_f}{c}(1-v_f) = \frac{E_f(1+v)}{E(1+v_f)}[Jc + 2Kc^3 v - \frac{M}{c^3} - \frac{2N}{c}(1-v)] \\ J_f c + (3-2v_f)K_f c^3 + \frac{M_f}{c^3} + \frac{N_f}{c}(2v_f - 1) = \frac{E_f(1+v)}{E(1+v_f)}[Jc + (3-2v)Kc^3 + \frac{M}{c^3} + \frac{N}{c}(2v-1)] \\ J_f + \frac{3M_f}{d^4} + \frac{2N_f}{d^2} = \frac{\sigma_H - \sigma_h}{2}(1 - \frac{a^2}{d^2})(1 - 3\frac{a^2}{d^2}) \\ J_f + 3K_f d^2 - \frac{3M_f}{d^4} - \frac{N_f}{d^2} = -\frac{\sigma_H - \sigma_h}{2}(1 - \frac{a^2}{d^2})(1 + 3\frac{a^2}{d^2}) \end{cases}$$

(B21)

The total stress equals to the sum of stresses in situation (i) and (ii).

APPENDIX C: THE EFFECT OF TEMPERATURE ON RADIAL AND HOOP STRESS

Figure C illustrates the radial and hoop stress distribution along the radius of the cement sheath at 0° and 90°. Tension is observed along hoop direction at 0° in the casing-cement interface when heat transfer from formation to casing ($\Delta T < 0$) (**Figure C-c**). Stresses in other locations with opposite heat transferring direction ($\Delta T > 0$) are compressive. For the radial stress, the magnitude in 90° is higher than 0°. Lower differential temperature in $\Delta T > 0$ condition or higher differential temperature in $\Delta T \leq 0$ condition results increasing radial stress. For the hoop stress, the highest risk of stress exceeding compressive strength occurs in the casing-cement interface at 90° when $\Delta T > 0$ and differential temperature is high. Radial fracture is the most likely failure mode at 0° of the casing-cement interface with high differential temperature when $\Delta T \leq 0$.

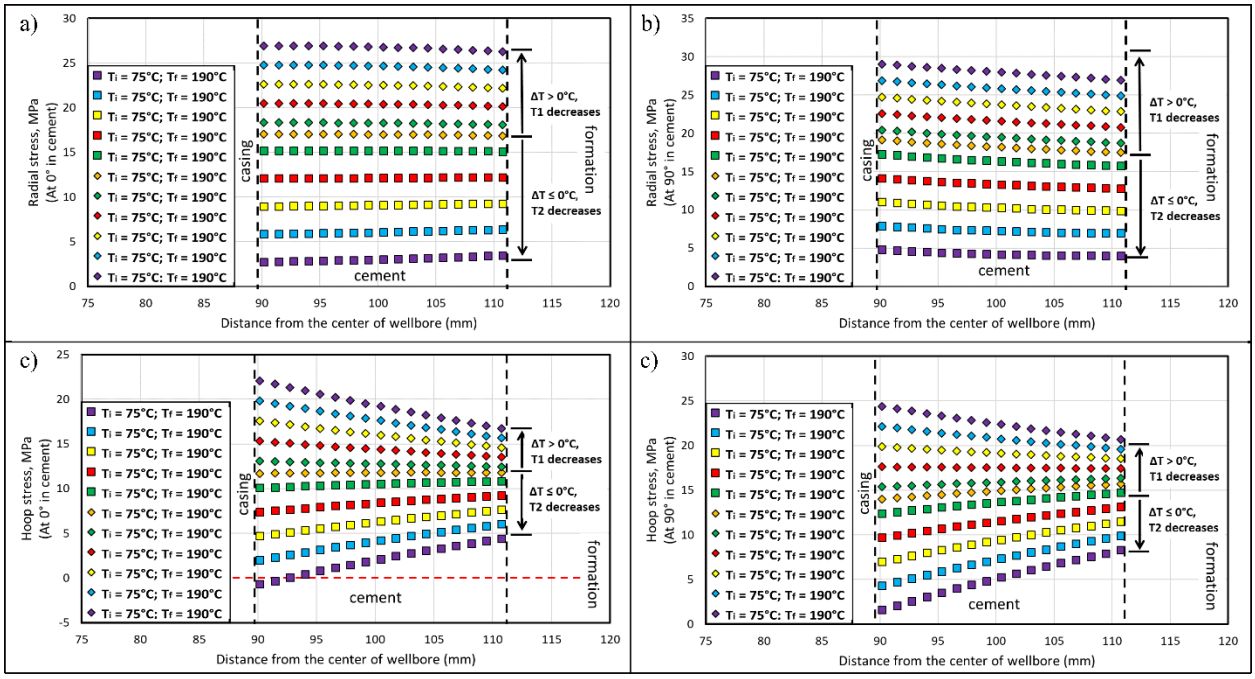

Figure B: Sensitivity response curve of variable differential temperatures. a) Radial stress at 0° within cement sheath. b) Radial stress at 90° within cement sheath. c) Hoop stress at 0° within cement sheath. d) Hoop stress at 90° within cement sheath.